



SCUOLA INTERNAZIONALE SUPERIORE DI STUDI AVANZATI

SISSA Digital Library

Nonlinearity accelerates the thermalization of the quartic FPUT model with stochastic baths

Original

Nonlinearity accelerates the thermalization of the quartic FPUT model with stochastic baths / Schmid, H.; Succi, S.; Ruffo, S. - In: JOURNAL OF STATISTICAL MECHANICS: THEORY AND EXPERIMENT. - ISSN 1742-5468. - 2021:5(2021), pp. 1-15. [10.1088/1742-5468/abfcbc]

Availability:

This version is available at: 20.500.11767/127027 since: 2022-03-11T14:12:15Z

Publisher:

Published

DOI:10.1088/1742-5468/abfcbc

Terms of use:

Testo definito dall'ateneo relativo alle clausole di concessione d'uso

Publisher copyright

IOP- Institute of Physics

This version is available for education and non-commercial purposes.

note finali coverpage

(Article begins on next page)

Nonlinearity accelerates the thermalization of the quartic FPUT model with stochastic baths

Harald Schmid

Universität Regensburg, GER-93040 Regensburg, Germany

Scuola Normale Superiore, I-56126 Pisa, Italy

E-mail: haraldschmid777@gmail.com

Sauro Succi

Center for Life Nano Science @ La Sapienza, Italian Institute of Technology, I-00161

Roma, Italy

Scuola Normale Superiore, I-56126 Pisa, Italy

Stefano Ruffo

SISSA, Via Bonomea 265, I-34136 Trieste, Italy

INFN Trieste, I-34149 Trieste, Italy

Abstract. We investigate the equilibration process of the strongly coupled quartic Fermi-Pasta-Ulam-Tsingou (FPUT) model by adding Langevin baths to the ends of the chain. The time evolution of the system is investigated by means of extensive numerical simulations and shown to match the results expected from equilibrium statistical mechanics in the time-asymptotic limit. Upon increasing the nonlinear coupling, the thermalization of the energy spectrum displays an increasing asymmetry in favour of small-scale, high-frequency modes, which relax significantly faster than the large-scale, low-frequency ones. The global equilibration time is found to scale linearly with system size and shown to exhibit a power-law decay with the strength of the nonlinearity and temperature. Nonlinear interaction adds to energy distribution among modes, thus speeding up the thermalization process.

Keywords: Fermi-Pasta-Ulam-Tsingou, Equilibration time, Canonical ensemble, Langevin heat baths

1. Introduction

Thermalization in the Fermi-Pasta-Ulam-Tsingou (FPUT) model has attracted much attention since the original formulation of the problem [1, 2, 3]. In the weak coupling regime the system reaches equipartition on a timescale which depends as a power-law [4, 5, 6] on the energy density. In this work, we take a different approach by studying

the equilibration process ranging from the weak to the strong coupling regime. In particular, we explore the steady-state dynamics and the relaxation to steady-state of the quartic FPUT attaching stochastic Langevin baths to both ends of the chain. A detailed study of the nonlinear model in equilibrium conditions was performed in [7] by realizing the canonical setting in a textbook manner, considering a small part of the microcanonical system. We show that our description using Langevin baths proves to be a successful framework to simulate both equilibrium and non-equilibrium properties of the nonlinear model in a canonical setting. We find by numerical simulations of the stochastic equations that increasing the nonlinear coupling accelerates the approach to equilibrium. Even at high nonlinearity equilibrium is surprisingly characterized by quasi-equipartition of linear energy among Fourier modes and relaxation to equilibrium is faster for high-frequency modes. We derive analytically a compact representation of the equilibrium properties of the model, introducing a dimensionless scaling variable $\lambda k_B T$ with temperature of the baths T and coupling strength λ . The expressions obtained from the canonical partition function for equilibrium quantities, such as internal energy and nonlinear energy, are in satisfactory agreement with the numerical results of the stochastic model. The equilibration time is shown to be linear in the system-size for a sufficiently large number of oscillators and is probed as a function of coupling (temperature) at different temperatures (couplings). We find that both dependencies are well-fitted by a decaying power-law with exponent $-1/3$ across four decades in temperature.

2. The model

We consider the following extension to the quartic FPUT with N particles given by the Langevin equations [8]

$$\begin{aligned} \ddot{q}_j = & q_{j+1} + q_{j-1} - 2q_j + \lambda \left[(q_{j+1} - q_j)^3 - (q_j - q_{j-1})^3 \right] \\ & - \delta_{1,j} [\gamma \dot{q}_j - \eta_L(t)] - \delta_{N,j} [\gamma \dot{q}_j - \eta_R(t)], \end{aligned} \quad (1)$$

where the baths at the left and right edge (L, R) have the same temperature T

$$\langle \eta_a(t) \rangle = 0, \quad \langle \eta_a(t) \eta_b(t') \rangle = 2\gamma k_B T \delta_{a,b} \delta(t - t'), \quad a, b = \{L, R\}. \quad (2)$$

Fixed boundary conditions were imposed such that $q_0 = q_{N+1} = 0$. Initially, the position and momenta are plain for all sites, $q_j(0) = 0$ and $\dot{q}_j(0) = p_j(0) = 0$. For reasons of simplicity, the mass m and the spring constant of the harmonic interaction k are set to unity, i.e. $m = 1$ and $k = 1$. Having a physical realization of our system in mind [9, 10], we couple stochastic motion only to the edges of the chain. The Langevin approach for the baths is a special case of the general Markovian evolution of the baths where the reservoirs are not affected by the system at all. The particular choice of the baths provides a physical implementation of the thermostats compared with more efficient schemes like Nosé-Hoover baths [11, 12] which have been applied to determine probability distributions for canonical momenta [13]. The model without nonlinearity

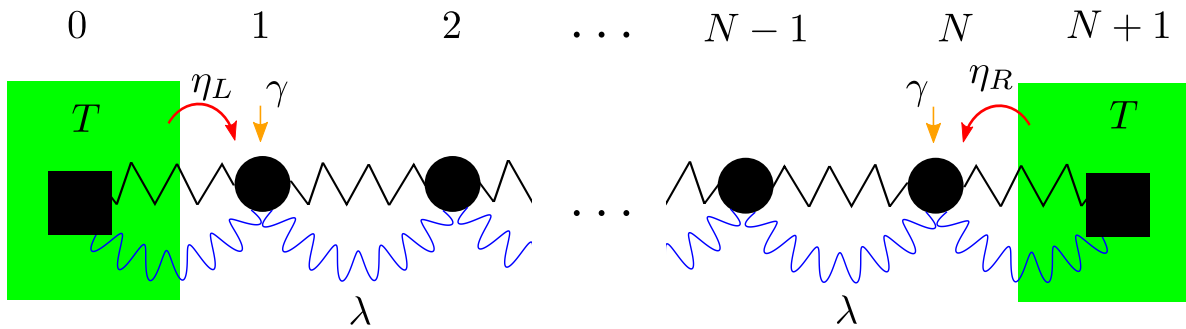


Figure 1. Sketch of the model (1). A chain of N particles with quadratic (black springs) and quartic interaction (blue whirls, coupling strength λ) is attached to stochastic baths of the same temperature T . The ends (0 and $N + 1$) are fixed.

($\lambda = 0$) coupled to Langevin baths is known to thermalize, i. e. all particles have equal kinetic energy as time goes to infinity [14, 15].

3. Numerical implementation

We have integrated the equations of motion using a standard fourth order Runge-Kutta scheme (RK4) for the deterministic part and a simple first order Euler–Maruyama method for the stochastic term [16]. Other integration schemes (e.g. Velocity-Verlet), have also been considered for the deterministic part, which proved to be slower at a comparable order of accuracy. Setting the dissipation to unity ($\gamma = 1$ fixed for the rest of the paper), a stepsize $\Delta t = 0.01$ proved to be stable and sufficiently accurate for the purpose of this paper. Considering the deterministic part separately ($T = 0$), the largest observed deviation from energy conservation using the RK4 scheme, was of the order of 10^{-9} , for the case of $N = 32$ sites and strong nonlinearity $\lambda = 10$. For the full stochastic system, equipartition was reached numerically and the fluctuation-dissipation theorem was satisfied within less than 1 % for the longest simulation times (5000 timesteps). Ensemble-averaging and time-averaging were implemented simultaneously for every quantity under inspection. In equations:

$$F(t) = \frac{1}{2\delta t} \sum_{l=1}^{N_{run}} \int_{t-\delta t}^{t+\delta t} ds f_l(s), \quad (3)$$

with $f_l(t)$ being a measured quantity for a single Wiener-process realization. Unless explicitly mentioned otherwise, we will refer from now on to every quantity F in the text as the averaged one. A window of $\delta t = 100$ and $N_{run} = 100$ runs are used for the statistics. Numerical errors appear due the choice of the timestep which affects predominantly the integration of the stochastic part, due to the low-order Euler-Mayurama scheme (time-integration is numerically more costly than ensemble-averaging since the latter can be run in parallel across independent tasks). We have checked the validity of our results by doubling the timestep, size of the ensemble and of the time-averaging window for the time-average, thus confirming satisfactory convergence of the

stochastic simulations. Higher order schemes for the stochastic part might improve the efficiency of the code and will be considered in the future for longer time simulations.

4. Time-evolution of the normal modes

The kinetic energy of a single site defines a temperature distribution in real space $k_B T_j(t) = \dot{q}_j^2(t)$. For the linear Langevin chain (recovered by setting $\lambda = 0$) all oscillators equilibrate to the temperature of the baths, i. e. $T_j(\infty) = T$ [14, 17]. We will show that this holds also for the nonlinear case. It is useful to introduce the normal modes of the harmonic system [18]

$$A_k(t) = \sqrt{\frac{2}{N+1}} \sum_{j=1}^N q_j(t) \sin\left(\frac{kj\pi}{2(N+1)}\right). \quad (4)$$

Their frequencies are $\omega_k = 2\sin(k\pi/(2N+2))$ and the linear energy is given by $E_k = 1/2(\dot{A}_k^2 + \omega_k^2 A_k^2)$. The total energy stored in the linear motion of the modes is $\sum_k E_k$. The probability to find the system in mode k is adopted according to [5, 19, 20]

$$p_k(t) = \frac{E_k}{\sum_k E_k}(t). \quad (5)$$

If the nonlinearity is weak the total energy E is well-approximated by the linear energy in the modes, i. e. $E \approx \sum_k E_k$. This is not true anymore for the strong coupling regime.

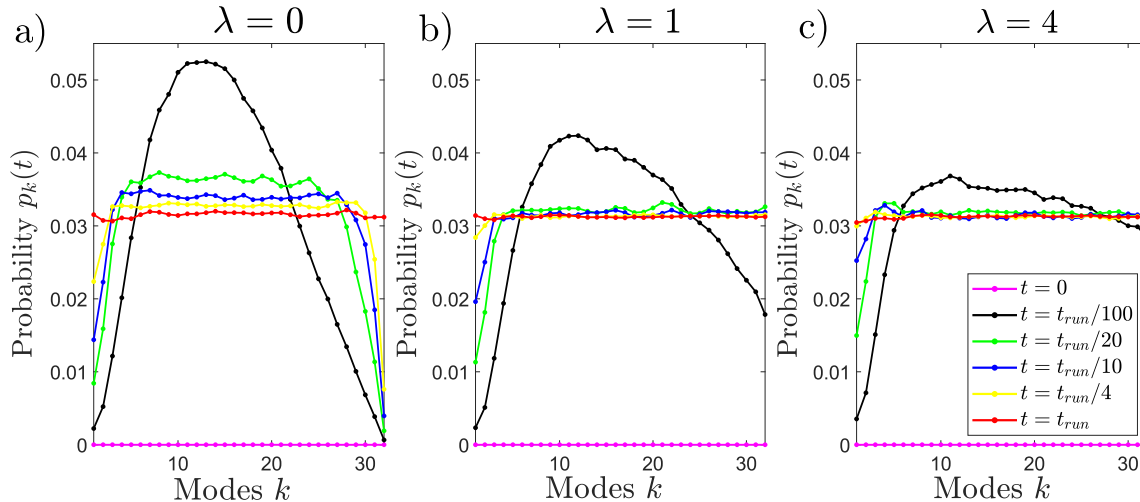


Figure 2. Distribution of modes (bath temperature $T = 1$, dissipation $\gamma = 1$). We evolved the system of $N = 32$ sites for $t_{run} = 5000$ and three different strengths of the nonlinearity λ until the distribution becomes flat due to equipartition. For the linear system ($\lambda = 0$) modes around $k \approx 12$ are excited early (black curve). The slowest and fastest modes reach equilibrium latest. Ramping up the coupling ($\lambda = 1, 4$) creates an asymmetry in the thermalization between modes at the ends of the spectrum as high-oscillating modes reach equilibrium faster than low-oscillating modes. Furthermore, equipartition is reached faster for larger coupling due to the quicker distribution of energy into modes at both ends of the spectrum.

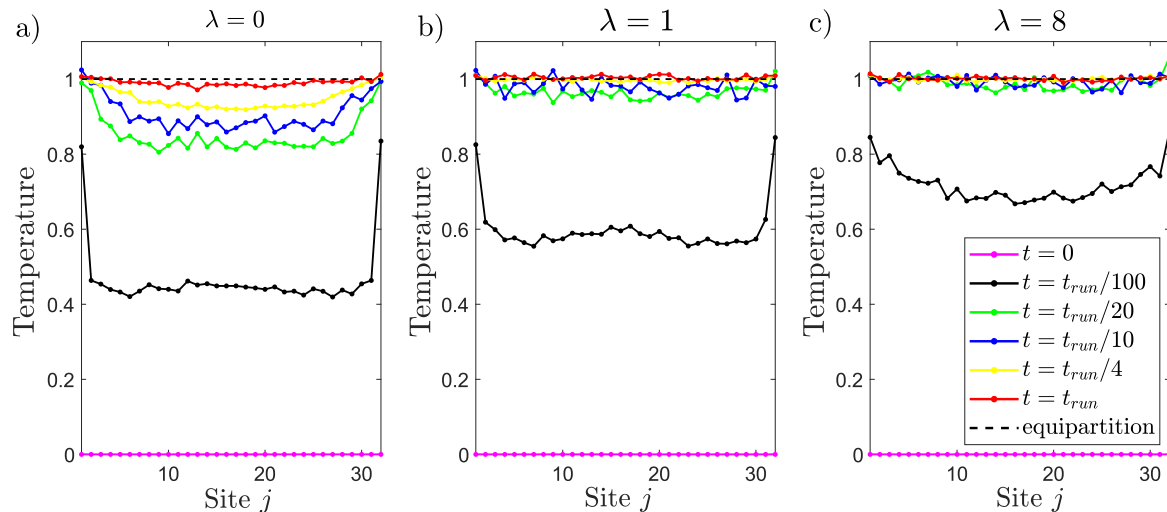


Figure 3. Temperature profiles $T_j(t)$ (same parameters as in figure 2). Equipartition is reached faster for larger coupling.

Nevertheless, (5) defines the probability distribution of the normal modes at every value of the coupling, and is properly normalized by $\sum_k E_k$. Excluding an anharmonic term from the definition gives us a clear perspective on the modification of the spectrum when the coupling is changed. We observe that the nonlinearity has an impact on the time evolution of the spectrum p_k .

Snapshots of temperature profiles $T_j(t)$ and the distribution of modes $p_k(t)$ for different coupling strengths are shown at different points during their evolution in figure 2 and 3. For the latest time in our simulation, the system approaches a homogeneous temperature in real space and a flat spectrum in mode space, regardless of the coupling strength. Comparing distributions/temperature profiles for different coupling strengths at the early points in the evolution, the nonlinearity accelerates the thermalization process. For the linear case ($\lambda = 0$), modes around $k \approx N/3$ are fastest excited at early stages in the evolution. In comparison with the real space evolution, the exterior sites $j = 1$ and $j = N$ attached to the baths are early excited. Low- and high-oscillating Fourier modes at the ends of the spectrum reach equipartition latest and nearly at the same time. Ramping up λ , an asymmetry in the spectrum is observed, as high-oscillating modes are quicker to reach equipartition than the low ones. At $\lambda = 4$ (figure 2 c)), the first snapshot in the evolution (black curve) displays a spectrum which is almost flat for modes $k > 8$ and steeply declines for low-oscillating modes. The high-oscillating modes approach equilibrium on the same time scale as the fastest relaxed modes whereas low modes trail behind.

5. Thermodynamics from the stochastic model

Next, we derive analytic expressions for the internal energy, and the nonlinear and harmonic part of the energy in equilibrium. They are required to validate the

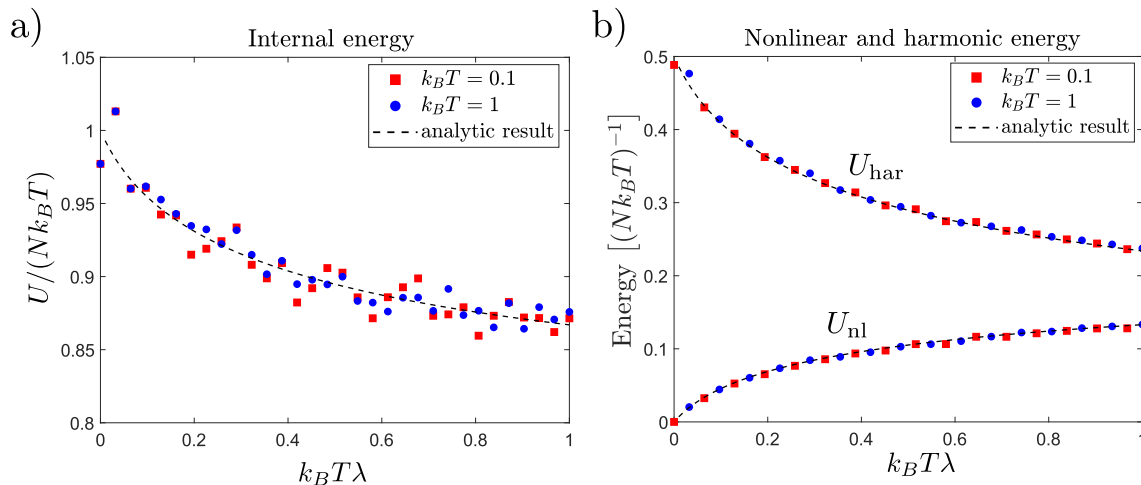


Figure 4. Dependence of the energy of the quartic FPUT in equilibrium ($N = 32$ sites). a) The internal energy normalized by the thermal energy of a linear chain, i.e. $U/(Nk_B T)$, is a function only of the product $k_B T \lambda$. The simulation using the stochastic baths agrees with the analytic result (10). b) Nonlinear energy U_{nl} increases with coupling while the harmonic energy U_{har} decreases (17) (black dotted).

corresponding time-asymptotic quantities in the simulation of the stochastic quartic FPUT. The partition function for the system reads

$$Z = \int \prod_{j=1}^N dp_j dq_j \exp \left\{ - (k_B T)^{-1} \left[\sum_{j=0}^N \frac{1}{2} p_j^2 + \frac{1}{2} (q_{j+1} - q_j)^2 + \frac{\lambda}{4} (q_{j+1} - q_j)^4 \right] \right\} \quad (6)$$

with momenta p_j and $p_0 = p_{N+1} = 0$ as well as $q_0 = q_{N+1} = 0$. Singling out the kinetic term we make the coordinate transformation [7]

$$\phi_L = q_1 - q_0, \quad \phi_1 = q_2 - q_1, \quad \dots, \quad \phi_{N-1} = q_N - q_{N-1}, \quad \phi_N = q_{N+1} - q_N, \quad \phi_R = q_{N+1}. \quad (7)$$

The variables ϕ_L and ϕ_R are not real coordinates but parameters due to the fixed boundaries. The Jacobian of the transformation is invertible and has determinant equal to the identity. The partition function is transformed to

$$Z = \xi(N) (\pi k_B T)^{N/2} \int \prod_{j=1}^N d\phi_j \exp \left\{ - (k_B T)^{-1} \sum_{j=0}^N \left[\frac{1}{2} \phi_j^2 + \frac{\lambda}{4} \phi_j^4 \right] \right\}, \quad (8)$$

displaying the same contribution of every variable ϕ_j . The prefactor $\xi(N) = \exp\left(-\frac{(q_0 - q_1)^2}{N+1}\right) / \sqrt{N+1}$ is a relict of the transformation and does not depend on the coordinates due to the fixed boundary conditions. The integral of the quartic exponential is found in terms of modified Bessel functions of the second kind $K_\nu(z)$. The partition function becomes

$$Z = \xi(N) \left[\frac{\pi k_B T}{2\lambda} \exp\left(\frac{1}{8k_B T \lambda}\right) K_{\frac{1}{4}}\left(\frac{1}{8k_B T \lambda}\right) \right]^{N/2}. \quad (9)$$

This is equivalent to the result given in [7] by the relation of the parabolic cylinder functions $D_\nu(y)$ and the Bessel functions $D_{-1/2}(y) = \sqrt{y/(2\pi)} K_{1/4}(y^2/4)$, upon

changing from fixed to periodic boundary conditions.

The internal energy is related to the partition function by $U = k_B T^2 \partial/\partial T \log(Z)$. We obtain

$$U = \frac{Nk_B T}{4} + \frac{N}{8\lambda} \mathcal{K} \left(\frac{1}{8k_B T \lambda} \right), \quad (10)$$

where we have defined the ratio of the Bessel functions

$$\mathcal{K}(y) = \frac{K_{\frac{5}{4}}(y)}{K_{\frac{1}{4}}(y)} - 1. \quad (11)$$

Again, the result is equivalent to [7]. Dividing in (10) by $k_B T$, the internal energy has a dimensionless scale $z = 8k_B T \lambda$

$$\frac{U}{Nk_B T}(z) = \frac{1}{4} + \frac{1}{z} \mathcal{K} \left(\frac{1}{z} \right). \quad (12)$$

The coupling λ plays by the found relation for z the role of an inverse nonlinear temperature scale. It is also worth investigating the harmonic part and nonlinear part of the energy

$$U_{\text{har}} = Z^{-1} \int \prod_{j=1}^N dp_j dq_j \sum_{j=0}^N \frac{1}{2} (q_{j+1} - q_j)^2 \exp \left\{ - (k_B T)^{-1} H \right\}, \quad (13)$$

$$U_{\text{nl}} = Z^{-1} \int \prod_{j=1}^N dp_j dq_j \sum_{j=0}^N \frac{\lambda}{4} (q_{j+1} - q_j)^4 \exp \left\{ - (k_B T)^{-1} H \right\}, \quad (14)$$

where H is the Hamiltonian of the quartic FPUT. The change of variables (7) and rewriting by parameter differentiation yields

$$U_{\text{har}} = -\lambda k_B T \frac{\partial}{\partial \lambda} \log \left[\int d\phi \exp \left\{ - (k_B T)^{-1} \left(\frac{1}{2} \phi^2 + \frac{\lambda}{4} \phi^4 \right) \right\} \right]^N, \quad (15)$$

$$U_{\text{nl}} = -\lambda k_B T \frac{\partial}{\partial g} \Big|_{g=1} \log \left[\int d\phi \exp \left\{ - (k_B T)^{-1} \left(\frac{g}{2} \phi^2 + \frac{\lambda}{4} \phi^4 \right) \right\} \right]^N. \quad (16)$$

The result can again be given in dimensionless form

$$\frac{U_{\text{har}}}{Nk_B T}(z) = \frac{2}{z} \mathcal{K} \left(\frac{1}{z} \right) - 1, \quad \frac{U_{\text{nl}}}{Nk_B T}(z) = \frac{3}{4} - \frac{1}{z} \mathcal{K} \left(\frac{1}{z} \right). \quad (17)$$

Observe that $z^{-1} \mathcal{K}(z^{-1}) \rightarrow \frac{1}{2}$ for infinitely strong coupling $z \rightarrow \infty$, so the asymptotics is given by

$$\lim_{k_B T \lambda \rightarrow \infty} U = \frac{3}{4} N k_B T, \quad \lim_{k_B T \lambda \rightarrow \infty} U_{\text{nl}} = \frac{N}{4} k_B T, \quad \lim_{k_B T \lambda \rightarrow \infty} U_{\text{har}} = 0. \quad (18)$$

The asymptotic (and maximum) ratio of nonlinear energy U_{nl} and internal energy U settles at $U_{\text{nl}}/U = \frac{1}{3}$. The following ratio yields the contribution of nonlinear coupling to potential energy

$$\eta(z) = \frac{U_{\text{nl}}}{U_{\text{har}} + U_{\text{nl}}} = \frac{3z - 4 \mathcal{K}(z^{-1})}{4 \mathcal{K}(z^{-1}) - z}. \quad (19)$$

It assumes values on the unit interval, i.e. $\eta(0) = 0$ (purely linear) and $\eta(\infty) = 1$ (purely nonlinear), and thus provides a good measure to separate strong from weak coupling which we define by

$$\eta(z) \ll 1, \quad \text{weak coupling.} \quad (20)$$

We have simulated the linear case $\eta = 0$ up to values $\eta \approx 0.36$ (at $k_B T \lambda = 1$), covering both weak and strong coupling regime. The stochastic implementation of the canonical ensemble of the quartic FPUT shows quantitative agreement with the values of internal, linear and nonlinear energy expected from equilibrium statistical mechanics (see figure 4).

6. Equilibration time

Having assessed the equilibrium properties of the system, next we utilize the stochastic model to numerically investigate the dependence of the relaxation to steady-state on the system size, temperature and nonlinearity. We define the equilibration time t_{eq} as the minimum time for which the total energy $E(t)$ reaches the equilibrium energy $U = U(\lambda)$ (10) and stays around it within fluctuations of the order of a small fraction of $\sim k_B T$. Numerically, it is convenient to take a window $|E - U|/(k_B T N) < 1\%$ (illustrated in figure 5 b)).

For a given temperature T and coupling λ , we find that the equilibration time depends linearly on the system size, provided N is large enough, see figure 6. We have fixed

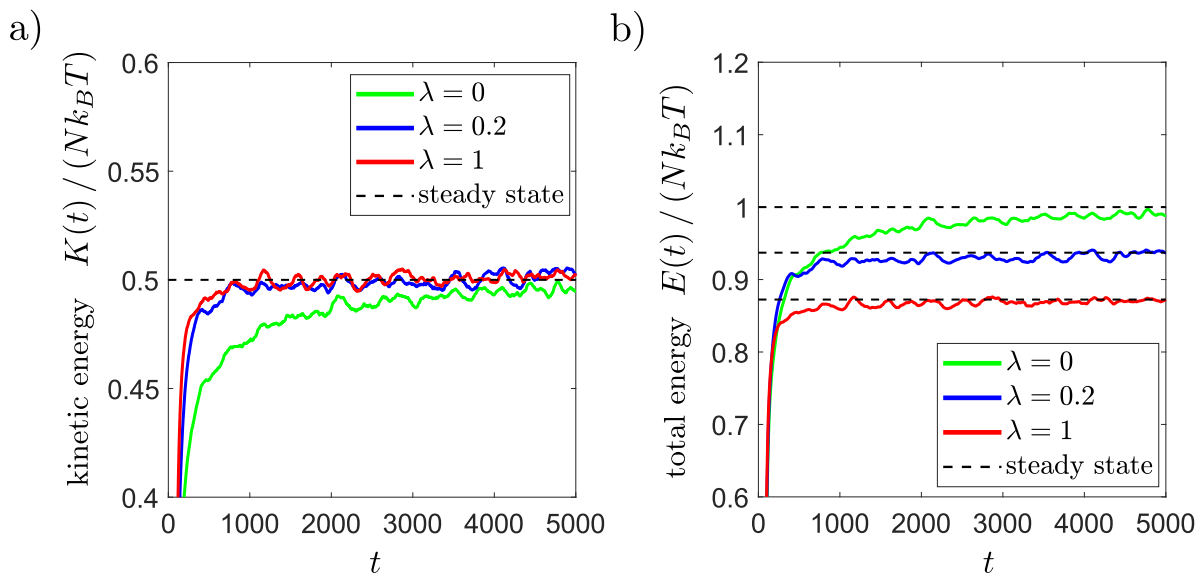


Figure 5. Equilibration of total kinetic energy $K(t) = \sum_j p_j^2/2$ and total energy $E(t)$ ($N = 32$, $k_B T = 0.1$). The straight (colored) lines are simulation for different strengths of the coupling while the black dotted lines display the value of the energy predicted from the partition function. The kinetic energy always reaches $Nk_B T/2$ independent of coupling, the total energy approaches $U(\lambda)$ and decreases with coupling. Nonlinearity accelerates the equilibration process.

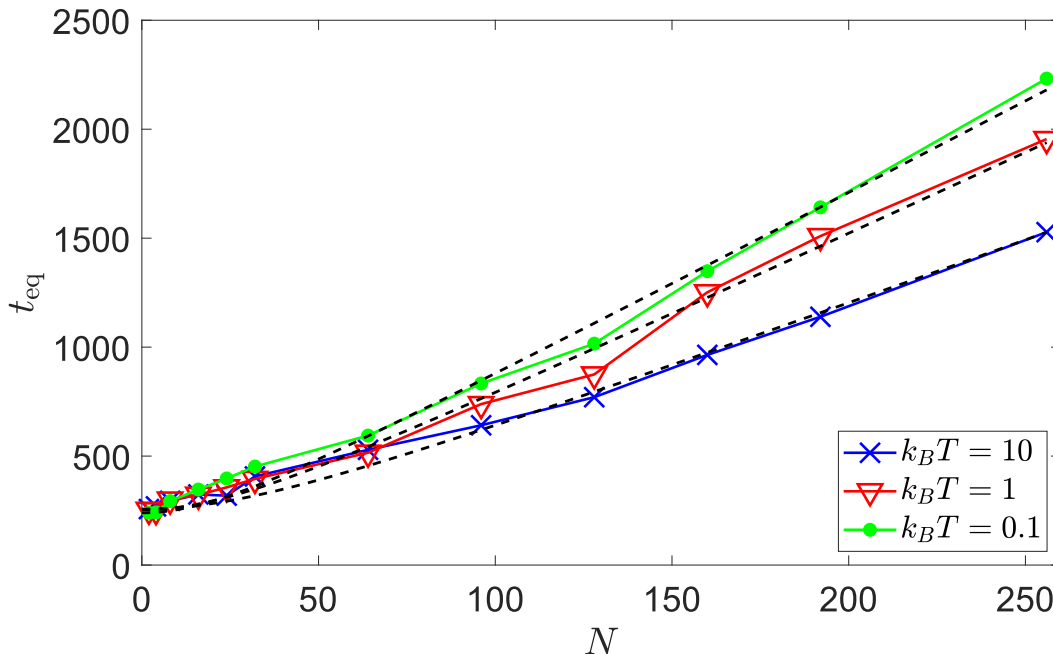


Figure 6. Dependence of the equilibration time on system size. The equilibration time is linear in the system size $t_{\text{eq}} \simeq \sqrt{t_0^2 + t_1^2 N}$ for N large enough (fixed $\lambda = 10$). The single-body relaxation time is $t_0 \approx 300$ in the plot. The slope depends on temperature $t_1 = t_1(T)$ and increases with decreasing T , explicitly $t_1(k_B T = 10) = 5.8$, $t_1(k_B T = 1) = 7.5$ and $t_1(k_B T = 0.1) = 8.4$.

$\lambda = 10$ (strong coupling) and plotted t_{eq} as a function of N for various temperatures, finding good agreement with the following fit (the numerical values of the parameters are given in Appendix Appendix A)

$$t_{\text{eq}}(N)|_{\lambda, T} \simeq \sqrt{t_0^2 + t_1^2 N^2}, \quad (21)$$

Besides being directly suggested by visual inspection of the numerical data, this fit also responds to a simple physical interpretation. Indeed, t_0 is associated to single-body relaxation time, while t_1 is the increment of t_{eq} due to the insertion of a single extra-node in the lattice chain. For large $N > 100$, a linear scaling is clearly observed, with coefficient $t_1 = t_1(T)$ depending on the temperature, but not on the coupling strength. The main outcome of this analysis is the linear dependence of t_{eq} on N .

Figure 7 reports the equilibration time t_{eq}/N as a function of the nonlinearity λ . For a given temperature, the curves for different N are equidistantly spaced, e.g. $t_{\text{eq}}(\lambda, N = 32)/32 - t_{\text{eq}}(\lambda, N = 64)/64 = \text{const.}$ indicating that t_1 depends only weakly on the nonlinear coupling. For the case of a few sites $N \rightarrow 1$, temperature (at fixed λ) has no effect on the equilibration time, as seen from the fact that all curves in the figure 6 merge into a single one for $N \rightarrow 1$).

The linear dependence of t_{eq} on the system size is the main result of the work. We have added a cubic nonlinearity to the quartic FPUT model (1) and performed

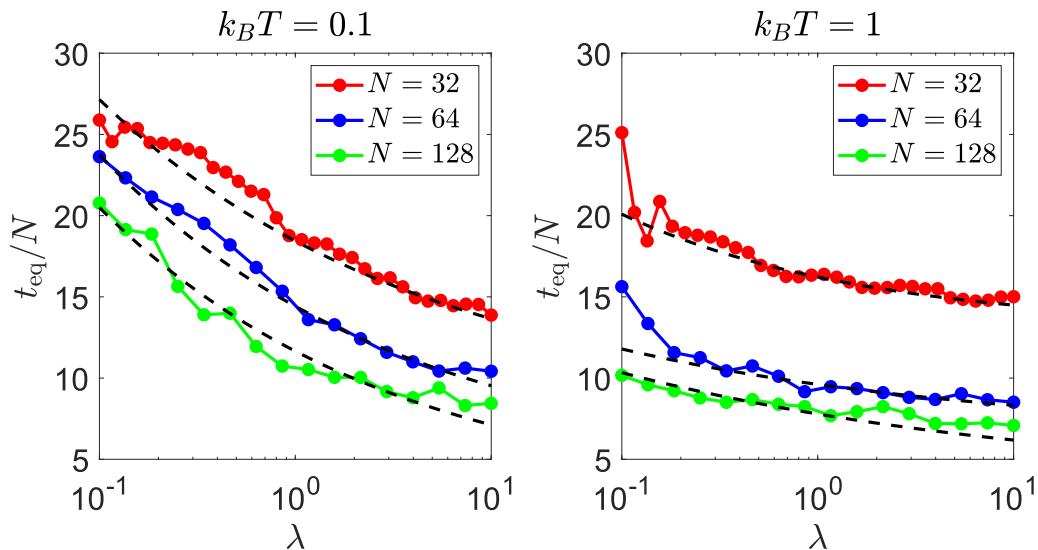


Figure 7. Dependence of the equilibration time on coupling. The equilibration has a power-law dependence on the coupling $\sim \lambda^{-\mu}$ with exponent μ in the range of $[0.23 - 0.35]$ for the shown graphs.

simulations to study $t_{\text{eq}}(N)$ for fixed λ and T (not shown in this paper). The linear relationship is still valid in this case, as long as the cubic nonlinearity is sufficiently weak to act as perturbation to the quartic model, namely as long as the potential displays a single minimum.

Next, we analyse the relaxation time as a function of temperature (see figure 8). The equilibration time decays weakly over a large range of simulated bath temperatures, and appears to be satisfactorily fitted by a power-law decay of the form:

$$t_{\text{eq}}(T)|_{N,\lambda} \simeq r_1 T^{-1/3} + r_0. \quad (22)$$

Fitting more generally $t_{\text{eq}} \simeq r_1 T^{-\nu} + r_0$, the exponent $\nu \approx 1/3$ is found for different

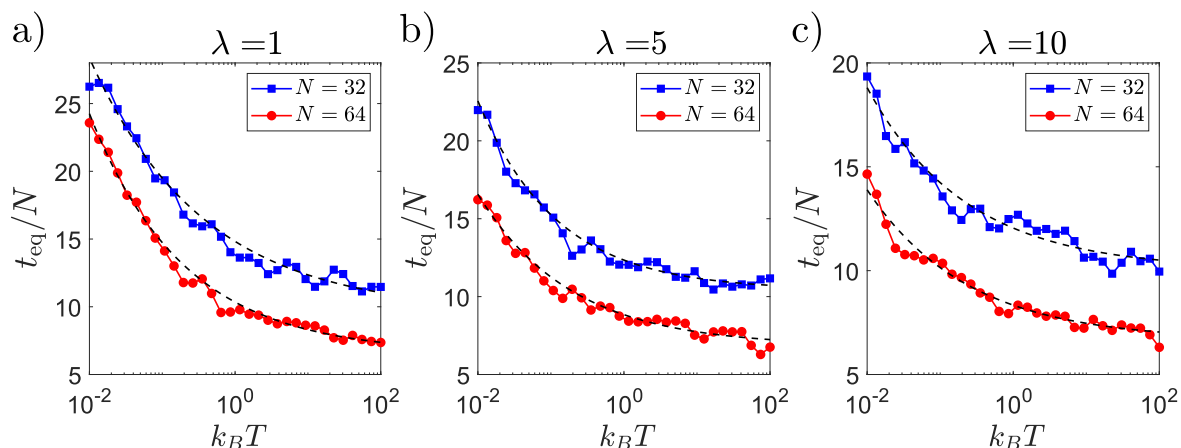


Figure 8. Dependence of the equilibration time on temperature. We find a power-law behavior $\sim T^{-1/3}$ for various coupling strengths and system sizes.

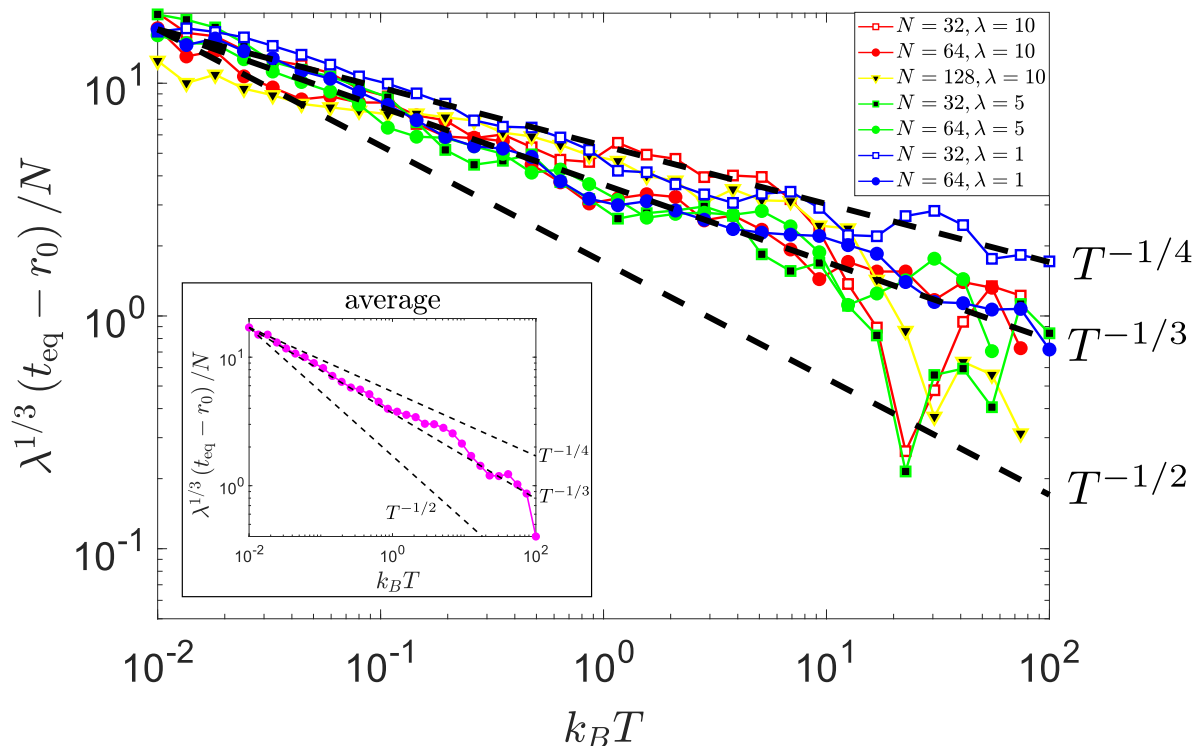


Figure 9. Equilibration time as a function of temperature for different couplings and system sizes. The equilibration time follows a power-law with exponent $T^{-1/3}$ over many orders of magnitude of the thermal energy. In the left bottom panel we show the average of all curves, assuming they all follow the suggested power-law.

couplings and system sizes (see Appendix A). The first parameter r_1 decays weakly with λ and increases linearly with N , as the two curves for $N = 32$ and $N = 64$ in each subfigure 8 a) - c) are almost equidistantly spaced. The second parameter r_0 is a sublinear function of N and numerically almost independent on λ , since the curves in figure 8 a) - c) (different λ , fixed N) have the same value for the largest bath temperature. We relate the parameters in (21) and (22) in the large N limit: the parameter r_0 takes numerically values similar to the case of the single-body relaxation time t_0 in our simulations at large N . By expanding (21) in N , we identify the term $t_1 N$ with $r_1 T^{-1/3}$, thereby deducing $t_1 \sim T^{-1/3}$.

At last, we investigate the effect of the coupling λ on the equilibration time. From the spectral time evolution (see figure 2), we have already observed that equilibration is accelerated by nonlinearity. As in the temperature-dependent study, t_{eq} depends weakly on λ , a power-law with a small exponent

$$t_{\text{eq}}(\lambda)|_{N,T} \simeq u_1 \lambda^{-1/3} + u_0. \quad (23)$$

We have again assumed first a general dependence like $t_{\text{eq}}(\lambda) \simeq u_1 \lambda^{-\mu} + u_0$, and concluded from our data that $\mu \approx 1/3$ (see Appendix A). The time-asymptotic value u_0 does not significantly depend on N , and increases with T , assuming numerically

comparable values like r_0 and t_0 . Again, we can indentify them in the large N -limit and relate u_0 to t_0 and r_0 , to give the leading contribution to the equilibration time in temperature (there might be also a contribution from u_0). It follows that t_0 and r_0 scale like $\sim \lambda^{-1/3}$.

The power-laws (22) and (23) can be motivated by dimensional analysis. The quantity

$$\omega_{\text{nl}} = (\lambda k_B T)^{1/4} m^{-1/2} \quad (24)$$

has the dimension of a inverse time. This suggests that if the equilibration time depends like a power-law on λ , then it should also depend like a power-law on T with the same exponent, and vice versa. Like in thermal equilibrium, λ plays the role of an inverse temperature. The other time-scales in the problem are the inverse dissipation constant, multiplied by the mass $\tau = \gamma/m$ and the harmonic frequency $\omega_{\text{har}} = \sqrt{k/m}$. The simulations provide strong evidence for a behavior of the form $t_{\text{eq}} \sim (\lambda T)^{-1/3}$, see figure 9, hence the nonlinear frequency enters like $t_{\text{eq}} \sim \omega_{\text{nl}}^{-4/3}$.

7. Discussion and conclusion

We have implemented the quartic FPUT model and succesfully reproduced the equilibrium canonical ensemble using Langevin baths. The equilibrium energy of our numerical approach agrees with the internal energy expected from the canonical ensemble (cf. figure 4). By an exact integration of the partition function of the nonlinear chain, we have been able to recover non-perturbative results from statistical mechanics, covering both weak and strong coupling regimes. Numerical integration of the stochastic differential equations matched the expression of the internal, nonlinear energy and harmonic energy from statistical mechanics in the time-asymptotic limit.

It was found that the mentioned components of the equilibrium energy of the quartic FPUT, normalized to the thermal energy in a linear chain, depend only on the product of temperature and coupling via the dimensionless scaling $z = 8k_B T \lambda$, i. e. $[U/(Nk_B T)](z)$. By the found scaling in z , we can make a proportionality argument: consider the potential of a single bond $V(\phi) = \frac{1}{2}\phi^2 + \frac{1}{4}\lambda\phi^4$ of the quartic FPUT and a change in coupling $\lambda \rightarrow 2\lambda$. The internal energy of the bond remains exactly the same if we cool down the bond by $T \rightarrow T/2$, regardless of the interaction strength, temperature of the baths and also system size. At equilibrium, all bonds feel the bath as if it was adjacent to them. The amount of nonlinearity η is likewise only a function of z , providing a closed formula (19) to distinguish quantitatively between the strong and weak coupling regimes.

Attaching the nonlinear system in the framework of Langevin baths puts us in the position to investigate the time evolution of the FPUT during the thermalization process. It is found that the nonlinearity accelerates equipartition, although not to a dramatic extent. This becomes clear from comparing the classic FPUT with the harmonic chain in terms of energy distribution. In the harmonic chain, energy is kept only in the intially excited mode, whereas in the FPUT case, energy is distributed among

all modes (provided at least one even and odd modes are initially excited in the quartic FPUT). When thermal baths are attached to the nonlinear FPUT, energy equipartition is reached through the Langevin terms under the presence of nonlinearity, while in the linear chain, this is obtained solely by the action of the Langevin terms.

Nonlinear interaction adds to energy distribution among modes, thus speeding up the thermalization process. This happens selectively in different regions of the spectrum. Energy is faster channeled to the high modes as the coupling is amplified. The equipartition time is a function of system size, temperature and coupling strength. For N large enough ($N > 100$), it increases linearly with the system size, with the slope dependent on temperature but not on the coupling strength. The relaxation time is increased by increasing the temperature of the baths and displays a power law behavior with exponent $-1/3$. Increasing the coupling λ leads to quicker equilibration, following again power-law dependence, with approximately the same exponent.

In a future work, the faster distribution of energy, favoring high-oscillating modes, should be investigated by considering the transient solution of the mode equations. It would also be interesting to investigate the effect of dimensionality on the scaling of the equilibration time with system size. We hope that the stochastic implementation of the canonical ensemble presented in this paper can prove useful to study equilibrium and non-equilibrium properties of similar nonlinear models, such as the Toda chain.

Acknowledgments

This work is part of MUR-PRIN2017 project "Coarse-grained description for non-equilibrium systems and transport phenomena (CO-NEST)" No. 201798CZL whose partial financial support is acknowledged. One of the authors (SS) acknowledges funding from the European Research Council under the Horizon 2020 Programme Grant Agreement n. 739964 ("COPMAT"). HS was financially supported by the ERASMUS program and the Physics Advanced program of the Elite Network of Bavaria (University of Regensburg, Germany), and is grateful for the hospitality of the Scuola Normale Superiore.

Appendix A. Fitting parameters

We state fitting parameters used in figures 6, 7 and 8.

$k_B T$	0.1	1	10
t_1	8.4	7.5	5.8

Table A1. Fitting parameters for the dependence of the equilibration time on system size $t_{\text{eq}}(N) = \sqrt{t_0^2 + t_1^2 N^2}$ and $\lambda = 10$. The single-body relaxation time is $t_0 \approx 300$.

	$\lambda = 1$	$\lambda = 5$	$\lambda = 10$
$N = 32$	$r_1 = 168, r_0 = 306$ $\nu = 0.28$	$r_1 = 61.6, r_0 = 333$ $\nu = 0.39$	$r_1 = 64, r_0 = 321$ $\nu = 0.32$
$N = 64$	$r_1 = 242, r_0 = 420$ $\nu = 0.34$	$r_1 = 129, r_0 = 437$ $\nu = 0.34$	$r_1 = 107, r_0 = 426$ $\nu = 0.32$

Table A2. Fitting parameters for the dependence of the equilibration time on temperature $t_{\text{eq}}(T) = r_1 T^{-\nu} + r_0$. The exponent ν is nearly independent of λ and N , and close to $\frac{1}{3}$.

	$N = 32$	$N = 64$	$N = 128$
$k_B T = 0.1$	$u_1 = 340, u_0 = 250$ $\mu = 0.26$	$u_1 = 659, u_0 = 264$ $\mu = 0.28$	$u_1 = 1192, u_0 = 300,$ $\mu = 0.29$
$k_B T = 1$	$u_1 = 100, u_0 = 419,$ $\mu = 0.35$	$u_1 = 200, u_0 = 415,$ $\mu = 0.23$	$u_1 = 826, u_0 = 206,$ $\mu = 0.34$

Table A3. Fitting parameters for the dependence of the equilibration time on coupling $t_{\text{eq}}(\lambda) = u_1 \lambda^{-\mu} + u_0$.

References

- [1] Fermi E, Pasta P and Ulam S 1955 *Studies of nonlinear problems* Tech. rep. Los Alamos Scientific Lab., N. Mex.
- [2] Gallavotti G 2007 *The Fermi-Pasta-Ulam problem: a status report* vol 728 (Berlin, Heidelberg: Springer Verlag)
- [3] Berman G P and Izrailev F M *The Fermi-Pasta-Ulam problem: Fifty years of progress* 2005 *Chaos* **15** 015104
- [4] Benettin G, Christodoulidi H and Ponno A *The Fermi-Pasta-Ulam Problem and Its Underlying Integrable Dynamics* 2013 *J. Stat. Phys.* **152** 195–212
- [5] Onorato M, Vozella L, Proment D and Lvov Y V *Route to thermalization in the α -Fermi-Pasta-Ulam system* 2015 *Proceedings of the National Academy of Sciences* **112** 4208–4213
- [6] Lvov Y V and Onorato M *Double Scaling in the Relaxation Time in the β -Fermi-Pasta-Ulam-Tsingou Model* 2018 *Phys. Rev. Lett.* **120** 144301
- [7] Livi R, Pettini M, Ruffo S and Vulpiani A *Chaotic behavior in nonlinear Hamiltonian systems and equilibrium statistical mechanics* 1987 *J. Stat. Phys.* **48** 539–559
- [8] Lepri S, Livi R and Politi A *Thermal conduction in classical low-dimensional lattices* 2003 *Physics Reports* **377** 1–80
- [9] *Experimental realization of Fermi-Pasta-Ulam-Tsingou recurrence in a long-haul optical fiber transmission system* 2019 *Scientific Reports* **9** 1–11
- [10] Pierangeli D, Flammini M and Zhang L e a 2019 *Fermi-Pasta-Ulam-Tsingou Recurrence in Spatial Optical Dynamics 2019 Conference on Lasers and Electro-Optics Europe & European Quantum Electronics Conference (CLEO/Europe-EQEC)* pp 1–1
- [11] Nosé S *A unified formulation of the constant temperature molecular dynamics methods* 1984 *The Journal of Chemical Physics* **81** 511–519
- [12] Hoover W G *Canonical dynamics: Equilibrium phase-space distributions* 1985 *Phys. Rev. A* **31** 1695–1697
- [13] Demirel M C and Sayar M *Statistical mechanics of Fermi-Pasta-Ulam chains with the canonical ensemble* 1997 *Phys. Rev. E* **55** 3727–3730
- [14] Rieder Z, Lebowitz J L and Lieb E *Properties of a Harmonic Crystal in a Stationary Nonequilibrium State* 1967 *J. Math. Phys* **8** 1073–1078
- [15] Kim S *Temperature profile and equipartition law in a Langevin harmonic chain* 2017 *J. Korean Phys. Soc.* **71** 264–268
- [16] Press W H, Teukolsky S A, Vetterling W T and Flannery B P 2007 *Numerical recipes* (Cambridge university press)
- [17] Nakazawa H *On the Lattice Thermal Conduction* 1970 *Progress of Theoretical Physics Supplement* **45** 231–262
- [18] Ford J *The Fermi-Pasta-Ulam problem: Paradox turns discovery* 1992 *Physics Reports* **213** 271–310
- [19] Livi R, Pettini M, Ruffo S, Sparpaglione M and Vulpiani A *Equipartition threshold in nonlinear large Hamiltonian systems: The Fermi-Pasta-Ulam model* 1985 *Phys. Rev. A* **31**(2) 1039–1045
- [20] Pistone L, Chibbaro S, Bustamante M, V Lvov Y and Onorato M *Universal route to thermalization in weakly-nonlinear one-dimensional chains* 2019 *Mathematics in Engineering* **1** 672–698